Wide-Band Dual Sense Circularly Polarized Resonant Cavity Antenna for X Band Applications

Swati Vaid[1], * and Ashok Mittal[2]

Abstract—This paper presents the design and analysis of a wideband circularly polarized resonant cavity antenna (RCA). The antenna structure consists of dual-layer Jerusalem cross type partially reflective surface (PRS) above a two-port wideband circularly polarized patch antenna. The PRS has been analyzed using equivalent circuit modeling. The PRS enhances the gain of the feeding patch antenna over wide range of frequencies. The structure provides left hand as well as right hand circular polarizations. Parametric analysis of the structure is also presented. The measured 10 dB return loss bandwidth and 3 dB axial ratio bandwidth of the RCA are 25% (8.24–10.63 GHz) and 28.8% (8.3 GHz–11.1 GHz), respectively. Isolation more than 10 dB is obtained for the frequency range 9.15–10.61 GHz. Measured results show peak realized gain of 9 dBi in the operating band.

1. INTRODUCTION

Circularly polarized (CP) antennas are used for various Radar applications, like ground penetrating Radars and vehicular Radars. These are mostly preferred because CP radiation can effectively overcome the effect of multi-path interference or fading. These types of antennas are also used for wireless and satellite applications, such as global navigation satellite systems (GNSS) [1], wireless sensors, and wireless local area networks. High gain and wide bandwidth are also desired in antennas used for high data rate wireless applications. Therefore, the research to design a high gain, wideband CP antenna is quite popular.

A smart solution to obtain high gain circularly polarized antennas is to use linearly polarized (or circularly polarized) planar antennas along with circular polarizers (or simple structures such as reflectors [2, 3] and superstrates [4–15]). The antenna configuration consisting of partially reflecting superstrates placed over planar antenna is known as resonant cavity antenna (RCA). Circularly polarized RCA structures are lighter in weight and smaller in size than conventional helical or horn antennas and thus provide a better solution for the applications mentioned above.

Circularly polarized RCAs have been reported in the literature by using two different methods [4]. In the first method, a circular polarizer made up of partially reflecting surface (PRS) had been used as the superstrate above a simple linearly polarized (LP) antenna. The polarizers made up of multiple layers [5–7] or single layer [8, 9] have been used. Polarizers can also be formed by manipulating the phases of the superstrates and ground such that the phase difference between the two LP components becomes an odd multiple of 90 degrees [10–12]. Chiral metamaterials have also been widely used to implement devices that transform the polarization of incident electromagnetic waves from linear to circular [16–21].

In the second method, circularly polarized (CP) antenna had been used as a primary source, loaded with PRS superstrate that supported CP radiation [13]. An array of 9×9 metallic square patch superstrate had been employed above circularly polarized microstrip patch antenna by Vaidya et al. [14].

* Corresponding author: Swati Vaid (vaid2006@gmail.com).
[1] Inderprastha Engineering College, Ghaziabad, U.P, India. [2] Ambedkar Institute of Advanced Communication Technologies and Research, Delhi-31, India.

The patch antenna had been loaded with mechanically tuned shorting posts to change the polarization of antenna from LHCP to RHCP and vice versa. The overall area of the structure was $5\lambda_0 \times 5\lambda_0$ with peak gain of 17.3 dBi. The structure showed narrow axial ratio bandwidth of 2.5%.

RCAs are inherently narrow band antennas with limited directivity bandwidth. However, impedance bandwidth of the RCA is mainly dependent on the primary feed and superstrate height. Also, the directivity/gain bandwidth of the RCA can be increased by using PRS superstrate with positive reflection phase gradient [22, 23]. Wideband circularly polarized primary feed with wide impedance bandwidth as well as superstrate with positive reflection phase gradient had been used in the literature to design wideband circularly polarized RCA.

Different topologies of wideband CP RCA have been reported in the literature [15, 24]. In [15] by Ju et al., the PRS had been formed by using square patch arrays with a pair of truncated corners, and it was placed above a sequentially rotated patch antenna array. The configuration provided right-handed CP and 6.8% axial ratio bandwidth with maximum gain of 21.1 dBi at 5.2 GHz over 1 dB bandwidth of about 4%. In [24] by Qin et al., a wide-band circularly polarized Fabry-Perot antenna had been designed with two-layer partially reflecting surface. The reported PRS was used above a wideband circularly polarized feeding antenna. The feeding antenna was formed by using a circular patch antenna fed by quasi-L strips, coupled feeding lines, Wilkinson power divider and a broadband 90 deg. phase shifter. This antenna achieved a 3-dB gain bandwidth and axial ratio bandwidth of 28.3% from 8.8 to 11.7 GHz with the peak gain of 14.7 dBi.

It is interesting to note that the earlier reported wideband circularly polarized RCA structures had the capability to transmit/receive single polarization only (left hand circularly polarized (LHCP) or right hand circularly polarized (RHCP)). Analysis of these types of RCAs with dual polarization capabilities (LHCP and RHCP) has not been explored earlier. Therefore, this aspect of polarization diversity and wide bandwidth in CP RCA is explored in this work, and a dual-sense CP RCA is designed for X band Radar applications.

2. ANTENNA GEOMETRY

Figures 1(a)–(b) show the geometry and dimensional details of the proposed antenna structure. This structure is designed for X band Radar Applications.

2.1. PRS Superstrate

The partially reflecting superstrate consisting of two layers of Jerusalem cross type frequency selective surface with unequal dimensions of crosses is used in this structure. Each layer has 8×8 unit cells. The FSS layers are printed on RT duroid 5880 with thickness of 0.762 mm and dielectric constant of 2.2 (shown in Fig. 1). The periodicity of the unit cells is used with 6.5 mm in both the PRS layers (Layer 4–5). The height between the two PRS layers $t2$ is taken 3 mm. The dimensions of metallic crosses are kept equal to $p1 = 6$ mm, $p2 = 5.5$ mm, $p3 = 0.5$ mm, $p4 = 1.5$ mm. The dimensions of the PRS are optimized to achieve positive reflection phase gradient at 10 GHz center frequency. The analysis is explained in Section 3.

2.2. Feeding Antenna

The feeding antenna is $45°(\alpha)$ rotated inverted patch fed by 3 dB branch-line coupler using rectangular slots in the ground plane. The patch antenna and coupler are designed on Rogers RO3003 of 0.762 mm thickness and dielectric constant 3. The thickness between the inverted patch and ground plane with feeding slots $t1$ is kept at 2 mm. Detailed geometry parameters are shown in Fig. 1(b). The dimensions of the antenna are optimized for maximum 10 dB return loss bandwidth (RLBW) and 3 dB axial ratio bandwidth (ARBW) simultaneously. The optimized dimensions of the antenna are given in Table 1.

2.3. Resonant Cavity Antenna

The PRS is placed over the feeding antenna at a height h of 15 mm. The air gaps between the dielectrics are maintained using nylon spacers. The lateral size of the antenna is taken as 60 mm × 60 mm.
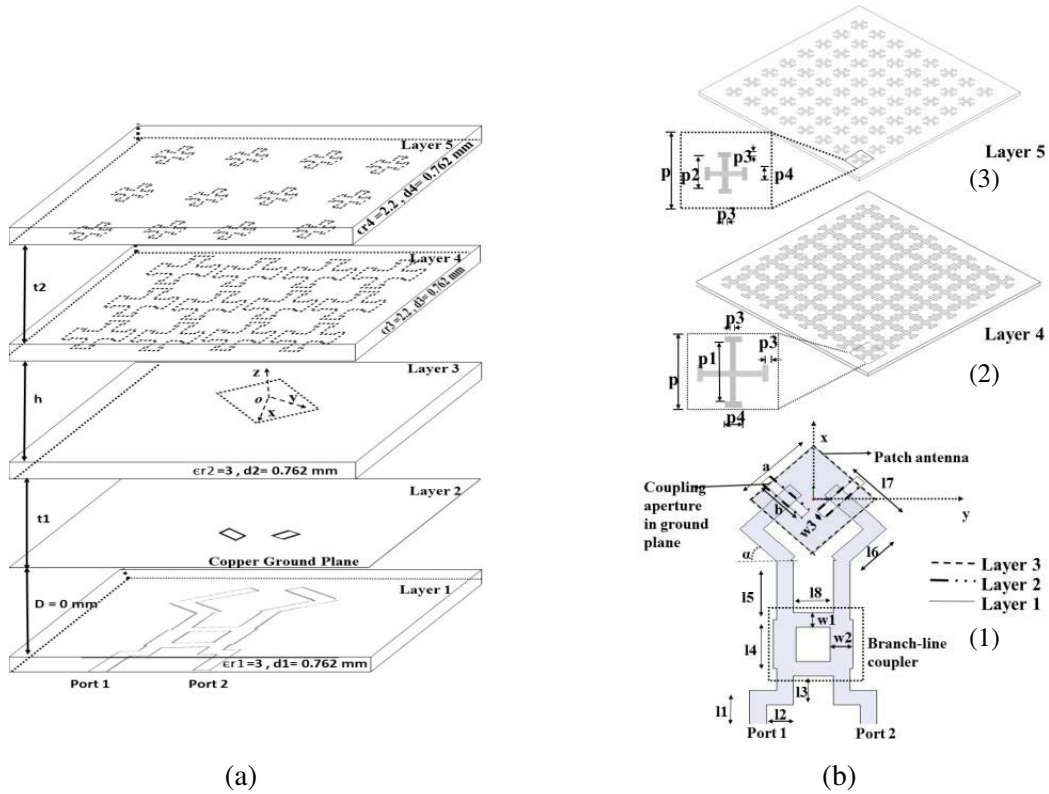
**Figure 1.** (a) Stacking details of the proposed antenna. (b) Dimensional details of the proposed structure.

Table 1. Optimized dimensions of the feeding antenna in mm.

Parameter	Value	Parameter	Value
$l1$	8.95	$l8$	5.12
$l2$	2.09	a	10
$l3$	3.54	b	6.5
$l4$	6.92	$w1$	1.91
$l5$	7.59	$w2$	2.6
$l6$	6.59	$w3$	1.2
$l7$	7.9		

3. ANTENNA ANALYSIS

3.1. PRS Superstrate

Dual layer Jerusalem cross type frequency selective surface (FSS) with dual linearly polarized feed was used in [25]. Same PRS is used as superstrate in the present work but with dual circularly polarized feed. This geometry is chosen because it can reflect the two orthogonal waves with nearly same characteristics and does not degrade the radiation performance of the antenna structure. The detailed analysis of this superstrate is given below. Infinite array of single arms of Jerusalem crosses (JC) can be modeled as series combination of inductance L and capacitance C (depicted in Fig. 2(a)) where L represents the storage of magnetic energy due the flow of current in the arms of Jerusalem crosses, and C represents the
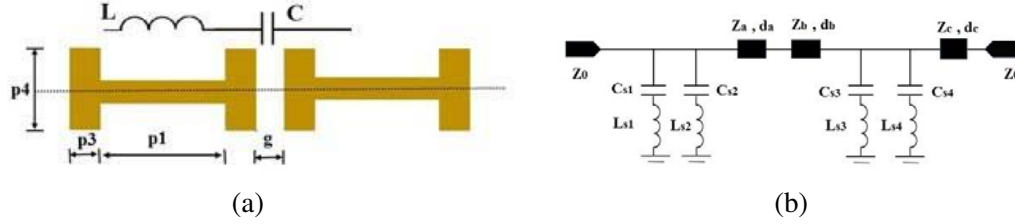
Figure 2. (a) Single arm of Jerusalem Cross with equivalent circuit elements. (b) Equivalent circuit of proposed PRS.

storage of electric energy in the gaps between the adjacent arms. These parameters can be calculated by the following expressions [26, 27],

$$L = \frac{Z_0 p_1}{c} \tag{1}$$

$$C = \frac{p_4}{\pi} \epsilon_0 \epsilon_{reff} \cosh^{-1} \left(\frac{2p_3}{g} \right) \tag{2}$$

Hence, an array of Jerusalem crosses can be modeled by parallel connection of two series L-C circuits representing each arm of the cross. The effect of variation of the dimensions of Jerusalem cross on parameters L and C is studied to understand the electromagnetic behavior of the FSS in detail. The parameter values obtained from Eqs. (1) and (2) are optimized with simulations. Table 2 shows the effect on L and Cv when arm length $p1$ is varied from 5 mm to 6 mm and the effect of varying $p4$ from 1 mm to 2.5 mm. It can be seen that increasing arm length $p1$ increases the inductance of FSS whereas it has negligible effect on capacitance. On the other hand, $p4$ increases both inductance and capacitance with each increment.

Table 2. Variation of equivalent inductance and capacitance of JC with $p1$ and $p4$.

$p1$ (mm)	L (nH)	C (pF)
5	1.68	0.019
5.25	1.77	0.0195
5.5	2.3	0.02
5.75	3.65	0.021
6	3.78	0.024
$p4$ (mm)	L (nH)	C (pF)
1	3.44	0.02
1.5	3.78	0.024
2	4.43	0.027
2.5	5.37	0.029

For the analysis of composite dual-layer PRS, the initial parameter values are calculated from Eqs. (1) and (2), and these values are then inserted in the ADS model and optimized, shown in Fig. 2(b). Series combinations of 'L_{s1}', 'C_{s1}' and 'L_{s2}', 'C_{s2}' in the circuit represent Jerusalem crosses on Layer 4 of the design, and series combinations of 'L_{s3}', 'C_{s3}' and 'L_{s4}', 'C_{s4}' are used for crosses on Layer 5. Z_0 shows the wave impedance in air. The transmission line sections between series networks of circuit elements represent dielectric layers upon which the metal patterns of PRS layers are printed with

impedance equal to Z_a, Z_c (i.e., wave impedance in the dielectric) and lengths equal to da and dc. Z_b (i.e., wave impedance in air) represents the air gap between two PRS layers.

The optimized values of the parameters obtained from ADS are $L_{s1} = 2.85\,\text{nH}$, $C_{s1} = 0.044\,\text{pF}$, $L_{s2} = 0.017\,\text{nH}$, $C_{s2} = 0.009\,\text{pF}$, $L_{s3} = 0.31\,\text{nH}$, $C_{s3} = 0.047\,\text{pF}$, $L_{s4} = 0.032\,\text{nH}$, $C_{s4} = 0.0036\,\text{pF}$ and $Za = Zc = 254\,\Omega$. Figs. 3(a)–(b) show the simulated linear plot and Smith chart of reflection coefficient at port 1. It is observed that this curve continuously travels clockwise along impedance transformation circles and conductance circles, and the positive slope of reflection phase is obtained.
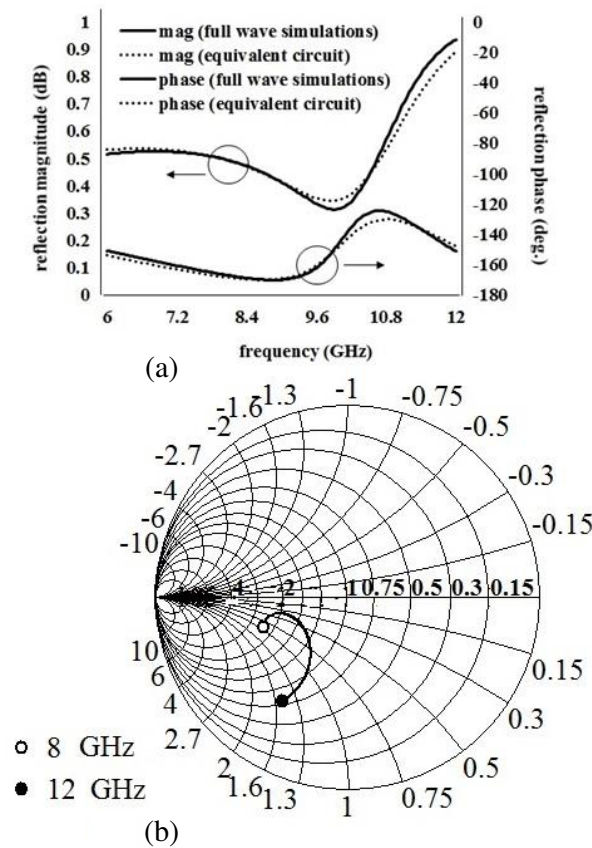
Figure 3. (a)–(b) Reflection coefficient of PRS in linear plot and smith chart.

3.2. RCA

For designing wideband circularly polarized resonant cavity antenna, the PRS can be designed using simulation study or the model discussed above for the required band, e.g., in this case X band is considered. The center frequency of the positive reflection phase gradient should coincide with the required band's center frequency. After that, the wideband circularly polarized microstrip antenna fed by branchline coupler is designed. The PRS is placed over this antenna at a height corresponding to the center frequency. The value of 'h' is optimized corresponding to the center frequency of 10 GHz and taken as 15 mm.

3.3. Parametric Analysis

3.3.1. PRS Superstrate

The effect of the variation in the dimensions of Jerusalem crosses on the reflection properties of double layer PRS was presented in [25].

3.3.2. RCA

Figures 4(a)–(b) show the simulated graph of axial ratio in the boresight direction versus frequency. There is insignificant change in the axial ratio of RCA, if the PRS parameters $t2$ is changed from 2.5 to 3.5 mm and $p4$ changed from 1 to 2 mm. Only the higher frequencies are affected. Therefore, this PRS will not degrade the performance of a well-designed circularly polarized feed antenna. Fig. 4(c) shows the effect of changing the height at which superstrate is placed over the isolation of the feeding ports. The height is changed from 14 mm to 18 mm. It can be seen that 10 dB isolation (S_{21}) bandwidth is a sensitive parameter, and it deteriorates with reducing height. At a height of 14 mm the isolation bandwidth splits into two bands.

Figures 4(d)–(e) show the simulated graph of surface current density over the Jerusalem crosses of PRS upper layer, for time phase φ varying from 0° to 270° with a step size of 90°. Fig. 4(d) shows the current density at 9 GHz, and Fig. 4(e) shows the current density at 10 GHz. It is observed that the currents on the PRS travel in clockwise direction with time phase when the signal is fed at port 1 of feeding antenna, and port 2 is port is terminated with 50 ohm load impedance. It can be observed that the current density vector is rotated 360 degrees in the clockwise direction as the time phase is progressed, suggesting the excitation of right hand circular polarization (RHCP). Left hand circularly polarized radiation (LHCP) can be obtained by feeding the antenna from port 2.

Figure 4(f) shows the variation in directivity with superstrate height h. It can be observed that the peak directivity drops by 2 dB with the increase of height from 14 mm to 18 mm. This drop in the directivity is attributed to the reduced intensity of reflection from the PRS when height is increased. It can be observed that height reduction will shift the peak directivity towards higher frequencies while increasing it will shift it to lower side.

# 4. EXPERIMENTAL RESULTS AND DISCUSSION

The proposed structure is fabricated and tested. The S parameters of the RCA are measured using Anritsu MS2038C VNA Master. Fig. 5(a) shows the reflection coefficient (S_{11}) of the proposed RCA configuration with 8×8 array of PRS unit cells, obtained at port 1 with the other port terminated with 50 ohm load impedance. The measured results are in close agreement with the simulated ones. The measured 10 dB return loss bandwidth of the RCA is 25% (8.24–10.63 GHz). Since the structure is symmetric with reference to the two feeding ports, the reflection coefficients are almost identical with minor differences.

Figure 5(b) shows the isolation (S_{21}) between the two feeding ports. Isolation more than 10 dB is obtained for the frequency range 9.15–10.61 GHz. A slight shift of frequency in the measured results is due to the fabrication tolerances.

The antenna pattern measurements have been performed by using the Star Lab setup from SATIMO Corporation. It is a fully automated setup which acquires both co-pol and cross pol components of the radiation pattern and computes the axial ratio from cross pol. In this setup, a Vector Network Analyzer (VNA) is used as the RF source/receiver for antenna measurements. The VNA is connected to the control unit which drives the two positioning motors and the electronic scanning of the probe array over the antenna under test.

Figures 6(a) and 6(b) show the simulated and measured normalized radiation patterns in *xoz*-plane and *yoz*-plane at 9 GHz when antenna is fed at port 1, and port 2 is port is terminated with 50 ohm load impedance. The elevation angle θ is varied from -180 to 180 degrees. LHCP component is more than 16 dB down from RHCP component at 9 GHz (boresight) in *xoz* plane, and it is more than 18 dB down in *yoz* plane. The discrepancy between the measured and simulated results is due to fabrication tolerances and alignment of various layers during assembly process. The main beam is slightly deflected in both the planes because of the presence of PRS-FSS superstrate, and supporting dielectric material for FSS.

Figure 6(c) shows the compared graphs of simulated and measured axial ratios of the composite structure (patch with PRS) in *xoz* plane. Similar results are also observed in *yoz* plane. The proposed structure exhibits axial ratio bandwidth of 28.8% (8.3 GHz–11.1 GHz). Measured and simulated axial ratios are in close agreement.
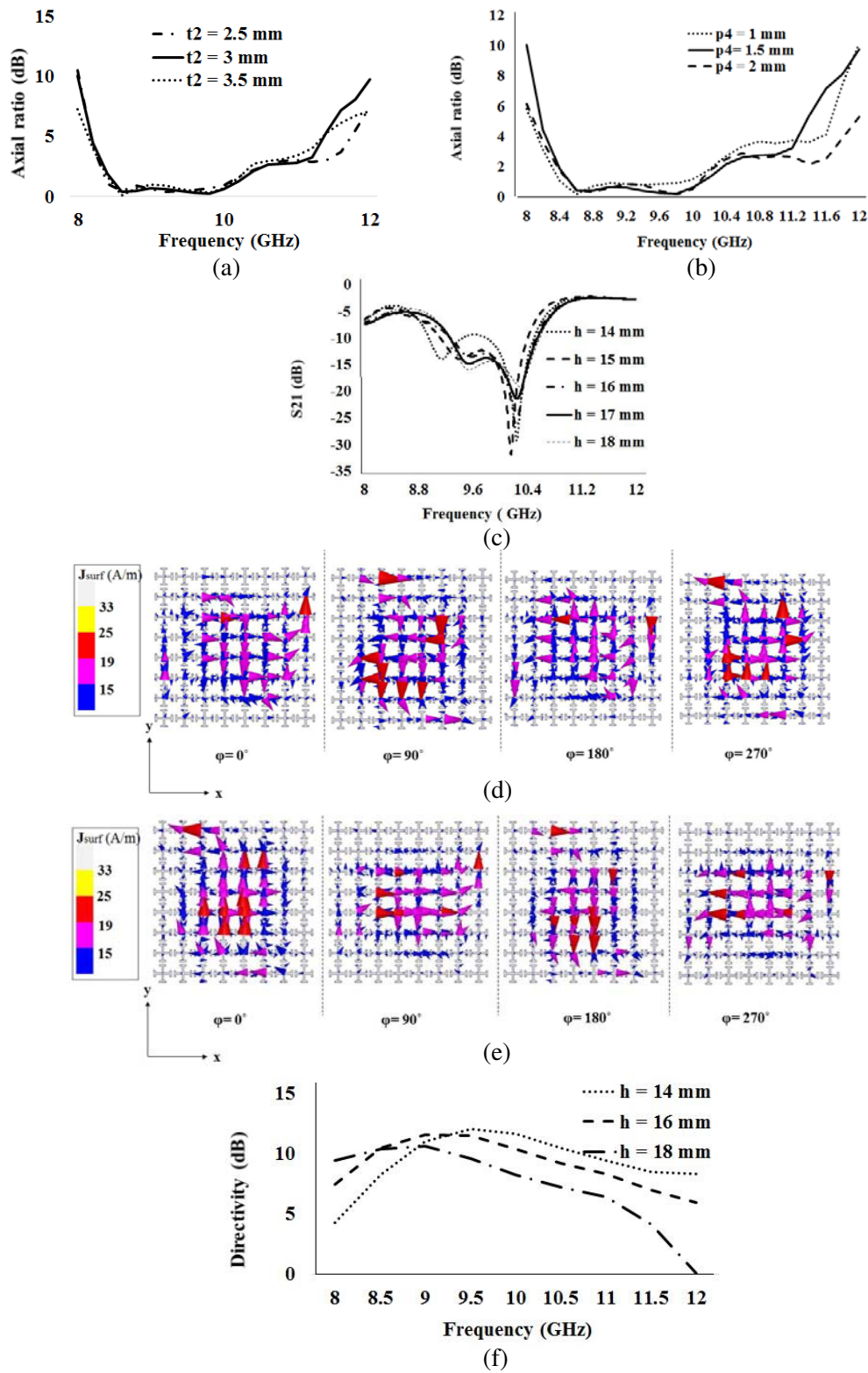
Figure 4. (a) Variation in axial ratio by changing $t2$. (b) Variation in axial ratio by changing $p4$. (c) Variation in S_{21} by changing height h. (d) Surface current density on PRS upper layer at 9 GHz. (e) Surface current density on PRS upper layer at 10 GHz. (f) Variation in the directivity by changing height h.
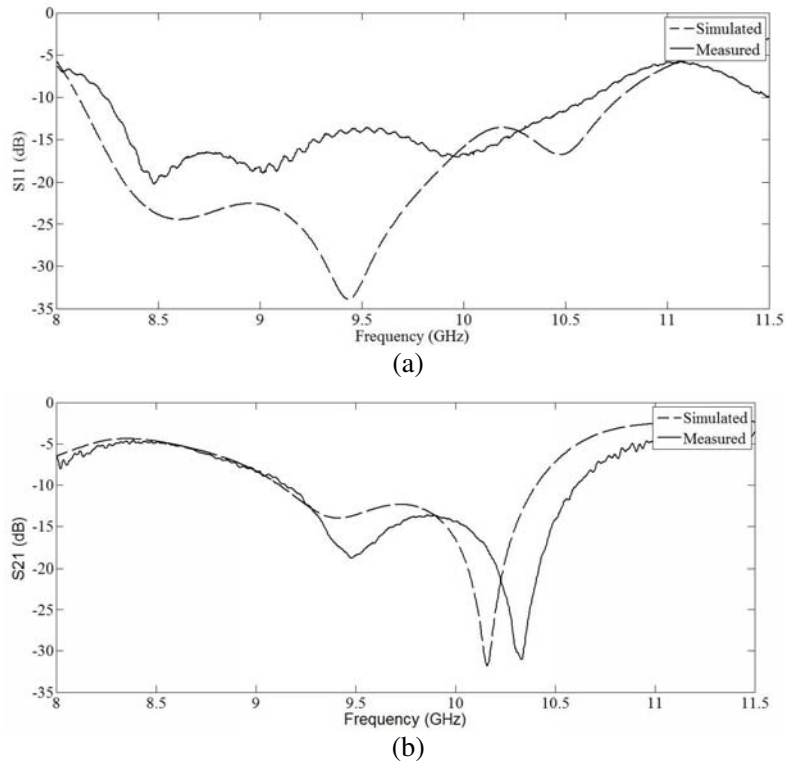
Figure 5. (a) Measured and simulated S_{11} of the proposed antenna structure. (b) Measured and simulated S_{21} of the proposed antenna structure.

(d)
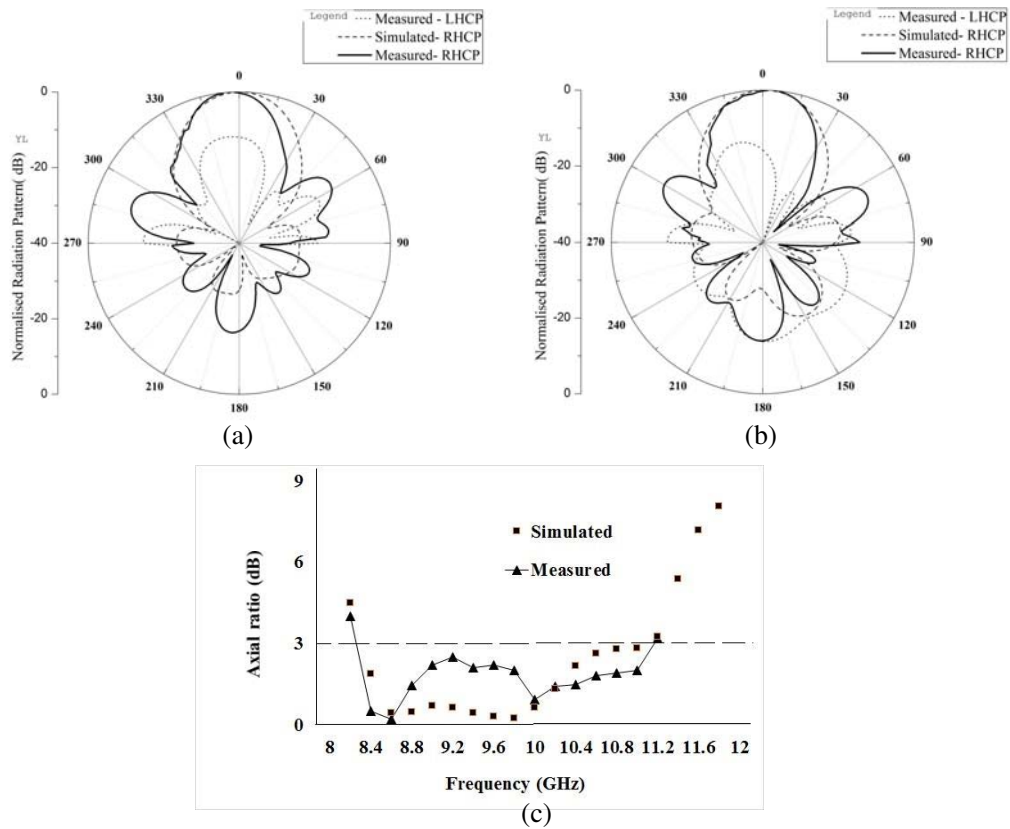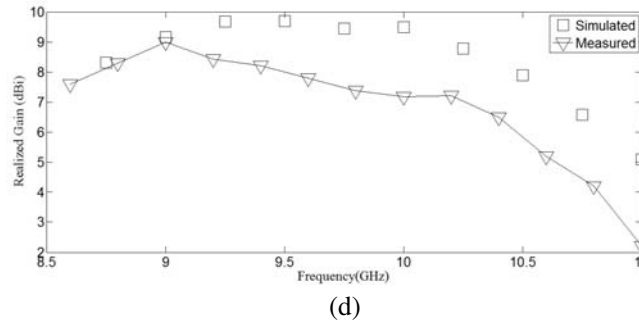
Figure 6. (a) Simulated and measured radiation pattern at 9 GHz (xoz plane). (b) Simulated and measured radiation pattern at 9 GHz (yoz plane). (c) Simulated and measured axial ratio versus frequency for the RCA configuration. (d) Measured and simulated gain versus frequency for the RCA configuration.

The simulated bore-sight realized gain of the proposed configuration is compared with the measured gain and shown in Fig. 6(d), for the entire operating band from 8.5–11 GHz. It can be seen that the maximum gain of 9 dBi is obtained in the entire band.

Table 3 shows the comparison of the present design with other RCA models reported in the literature. It is interesting to note that Jerusalem cross type FSS reflector has been reported earlier in the literature [3] for designing wideband circularly polarized and high gain antenna. In the referenced design, FSS reflector was used beneath wideband circularly polarized slot antenna for high gain applications. The structure showed impedance bandwidth of 74.3% and a 3-dB ARBW of 62%. The measured boresight gain of the proposed antenna was 3–4 dB higher than simple slot antenna, but the structure was designed with single circular polarization only. On the other hand, the present structure has ARBW and impedance bandwidth of 25% and 28.8%. The novelty of the design is that the antenna structure has polarization diversity, i.e., it is capable of producing right hand as well left hand circular polarization.

Table 3. 3-comparison with available literature.

Ref.	PRS	Size of RCA	ARBW (%)	Realized Gain (dB)	RCA Characteristic
[14]	Square patch	$5.5\lambda_0 \times 5.5\lambda_0 \times 0.5\lambda_0$	2.5	17.3	Mechanically tuned single feed RCA with dual polarization (RHCP and LHCP)
[15]	Square patch arrays	$5.5\lambda_0 \times 5.5\lambda_0 \times 0.5\lambda_0$	6.8	21.1	Single Polarization (RHCP or LHCP)
[24]	Double layer Patch	$2.13\lambda_0 \times 2.13\lambda_0 \times 0.67\lambda_0$	28.3	14.7	Single Polarization (RHCP or LHCP)
This Work	Double layer Jerusalem crosses	$2\lambda_0 \times 2\lambda_0 \times 0.7\lambda_0$	28.8	9	Dual feeding ports (RHCP and LHCP)

5. CONCLUSION

The design of a wideband dual circularly polarized resonant cavity antenna with double layer Jerusalem cross type partially reflective surface (PRS) as superstrate is presented in this paper. Full wave simulations and equivalent circuit model are used to understand the electromagnetic behavior of PRS. The structure exhibits 10 dB return loss bandwidth of 25% and isolation more than 10 dB for the frequency range 9.15–10.61 GHz. 3 dB axial ratio bandwidth of the RCA is 25% (8.24–10.63 GHz). Peak realized gain of the antenna structure is 9 dBi in the entire bandwidth.

REFERENCES

1. Maqsood, M., S. Gao, T. W. C. Brown, M. Unwin, R. De Vos Van Steenwijk, and J. D. Xu, "A compact multipath mitigating ground plane for multiband GNSS antennas," *IEEE Trans. Antennas Propag.*, Vol. 61, 2775–2782, 2013.

2. Ram Krishna, R. V. S., R. Kumar, and N. Kushwaha, "A circularly polarized slot antenna for high gain applications," *Int. J. Electron. Commun. (AEU)*, Vol. 68, 1119–1128, 2014.

3. Kushwaha, N. and R. Kumar, "Design of a wideband high gain antenna using FSS for circularly polarized applications," *Int. J. Electron. Commun. (AEU)*, Vol. 70, 1156–1163, 2016.

4. Vaid, S. and A. Mittal, "High gain planar resonant cavity antennas based on metamaterial and frequency selective surfaces," *Int. J. Electron. Commun. (AEU)*, Vol. 69, 1387–1392, 2015.

5. Diblanc, M., E. Rodes, E. Arnaud, M. Thevenot, T. Monediere, and B. Jecko, "Circularly polarized metallic EBG antenna," *IEEE Microw. Wirel. Compon. Lett.*, Vol. 15, 638–640, 2005.

6. Arnaud, E., R. Chantalat, M. Koubeissi, T. Monediere, E. Rodes, and M. Thevenot, "Global design of an EBG antenna and meander-line polarizer for circular polarization," *IEEE Antennas Wirel. Propag. Lett.*, Vol. 9, 215–218, 2010.

7. Chiu, S.-C. and S.-Y. Chen, "High-gain circularly polarized resonant cavity antenna using FSS superstrate," *IEEE Int. Symposium Antennas Propag. Society (APSURSI)*, 2242–2245, 2011.

8. Chiu, S.-C. and S.-Y. Chen, "Circularly polarized resonant cavity antenna using single-layer double-sided FSS superstrate," *IEEE Int. Symposium Antennas Propag. Society (APSURSI)*, 1–2, 2012.

9. Ma, X., C. Huang, M. Pu, C. Hu, Q. Feng, and X. Luo, "Single-layer circular polarizer using metamaterial and its application in antenna," *Microw. Opt. Technol. Lett.*, Vol. 54, 1770–1774, 2012.

10. Orr, R., G. Goussetis, and V. Fusco, "Design method for circularly polarized Fabry-Perot cavity antennas," *IEEE Trans. Antennas Propag.*, Vol. 62, 19–26, 2013.

11. Liu, Z.-G., Z.-X. Cao, and L.-N. Wu, "Compact low-profile circularly polarized Fabry-Perot resonator antenna fed by linearly polarized microstrip patch," *IEEE Antennas Wirel. Propag. Lett.*, Vol. 15, 524–527, 2016.

12. Muhammad, S. A., R. Sauleau, G. Valerio, L. Le Coq, and H. Legay, "Self-polarizing Fabry-Perot antennas based on polarization twisting element," *IEEE Trans. Antennas Propag.*, Vol. 61, 1032–1040, 2013.

13. Lee, D. H., Y. J. Lee, J. Yeo, R. Mittra, and P. Wee Sang, "Directivity enhancement of circular polarized patch antenna using ring-shaped frequency selective surface superstrate," *Microw. Opt. Technol. Lett.*, Vol. 49, 199–201, 2007.

14. Vaidya, A. R., R. K. Gupta, S. K. Mishra, and J. Mukherjee, "Right-hand/left-hand circularly polarized high-gain antennas using partially reflective surfaces," *IEEE Antennas Wirel. Propag. Lett.*, Vol. 13, 431–434, 2014.

15. Ju, J. and D. Kim, "Circularly-polarised high gain cavity antenna based on sequentially rotated phase feeding," *Electron. Lett.*, Vol. 49, 1198–1200, 2013.

16. Cao, T., Y. Li, X. Zhang, and Y. Zou, "Theoretical study of tunable chirality from graphene integrated achiral metasurfaces," *Photonics Research*, Vol. 5, No. 5, 441–449, 2017.

17. Cao, T., C. Wei, and Y. Li, "Dual-band strong extrinsic 2D chirality in a highly symmetric metal-dielectric-metal achiral metasurface," *Optical Materials Express*, Vol. 6, 303–311, 2016.

18. Cao, T., C. Wei, L. B. Mao, and S. Wang, "Tuning of giant 2D-chiroptical response using achiral metasurface integrated with graphene," *Optics Express*, Vol. 23, 18620–18629, 2015.

19. Cao, T., C. Wei, L. B. Mao, and Y. Li, "Extrinsic 2D chirality: Giant circular conversion dichroism from a metal-dielectric-metal square array," *Scientific Reports*, Vol. 4, 7442, 2014.

20. Cao, T., C. Wei, and L. Zhang, "Modeling of multi-band circular dichroism using metal/dielectric/metal achiral metamaterials," *Optical Materials Express*, Vol. 4, 1526–1534, 2014.

21. Cao, T. and M. J. Cryan, "Enhancement of circular dichroism by a planar non-chiral magnetic metamaterial," *Journal of Optics*, Vol. 14, 085101, 2012.

22. Wang, N., Q. Liu, C. Wu, L. Talbi, Q. Zeng, and J. Xu, "Wideband Fabry-Perot resonator antenna with two complementary FSS layers," *IEEE Trans. Antennas Propag.*, Vol. 62, 2463–2471, 2014.

23. Ge, Y., K. P. Esselle, and T. S. Bird, "The use of simple thin partially reflective surfaces with positive reflection phase gradients to design wideband, low-profile EBG resonator antennas," *IEEE Trans. Antennas Propag.*, Vol. 60, 743–750, 2012.

24. Qin, F., S. Gao, G. Wei, Q. Luo, C. Mao, C. Gu, J. Xu, and J. Li, "Wideband circularly polarized Fabry-Perot antenna," *IEEE Antennas Propag. Magazine*, Vol. 57, 127–135, 2015.

25. Vaid, S. and A. Mittal, "Wideband orthogonally polarized resonant cavity antenna with dual layer jerusalem cross partially reflective surface," *Progress In Electromagnetics Research C*, Vol. 72, 105–113, 2017.

26. Costa, F., A. Monorchio, and G. Manara, "Efficient analysis of frequency-selective surfaces by a simple equivalent-circuit model," *IEEE Antennas Propag. Magazine*, Vol. 54, 35–48, 2012.

27. Hosseini, M. and M. Hakkak, "Characteristics estimation for Jerusalem cross-based artificial magnetic conductors," *IEEE Antennas Wirel. Propag. Lett.*, Vol. 7, 58–61, 2008.